Periodogram and Discrete Fourier Transform

Property 4.2 The Spectral Density
If the autocovariance function, $\gamma(h)$, of a stationary process satisfies

$$\sum_{h=-\infty}^{\infty} |\gamma(h)| < \infty, \tag{4.10}$$

then it has the representation

$$\gamma(h) = \int_{-1/2}^{1/2} \mathrm{e}^{2\pi i\omega h} \, f(\omega) \, d\omega \quad h = 0, \pm 1, \pm 2, \ldots \tag{4.11}$$

as the inverse transform of the spectral density, which has the representation

$$f(\omega) = \sum_{h=-\infty}^{\infty} \gamma(h)\mathrm{e}^{-2\pi i\omega h} \quad -1/2 \leq \omega \leq 1/2. \tag{4.12}$$

Definition 1.14 *The* **sample autocovariance function** *is defined as*

$$\widehat{\gamma}(h) = n^{-1} \sum_{t=1}^{n-h} (x_{t+h} - \bar{x})(x_t - \bar{x}), \tag{1.34}$$

with $\widehat{\gamma}(-h) = \widehat{\gamma}(h)$ for $h = 0, 1, \ldots, n-1$.

Definition 4.1 *Given data $x_1, \ldots, x_n$, we define the* **discrete Fourier transform (DFT)** *to be*

$$d(\omega_j) = n^{-1/2} \sum_{t=1}^{n} x_t e^{-2\pi i\omega_j t} \tag{4.18}$$

for $j = 0, 1, \ldots, n-1$, where the frequencies $\omega_j = j/n$ are called the **Fourier** *or* **fundamental frequencies**.

$$x_t = n^{-1/2} \sum_{j=0}^{n-1} d(\omega_j)\mathrm{e}^{2\pi i\omega_j t} \tag{4.19}$$

for $t = 1, \ldots, n$.

Definition 4.2 *Given data* $x_1, \ldots, x_n$, *we define the* **periodogram** *to be*

$$I(\omega_j) = |d(\omega_j)|^2 \tag{4.20}$$

for $j = 0, 1, 2, \ldots, n-1$.

Note that $I(0) = n\bar{x}^2$, where $\bar{x}$ is the sample mean. In addition, because $\sum_{t=1}^{n} \exp(-2\pi i t \frac{j}{n}) = 0$ for $j \neq 0$,[6] we can write the DFT as

$$d(\omega_j) = n^{-1/2} \sum_{t=1}^{n} (x_t - \bar{x}) e^{-2\pi i \omega_j t} \tag{4.21}$$

for $j \neq 0$. Thus, for $j \neq 0$,

$$\begin{aligned} I(\omega_j) = |d(\omega_j)|^2 &= n^{-1} \sum_{t=1}^{n} \sum_{s=1}^{n} (x_t - \bar{x})(x_s - \bar{x}) e^{-2\pi i \omega_j (t-s)} \\ &= n^{-1} \sum_{h=-(n-1)}^{n-1} \sum_{t=1}^{n-|h|} (x_{t+|h|} - \bar{x})(x_t - \bar{x}) e^{-2\pi i \omega_j h} \\ &= \sum_{h=-(n-1)}^{n-1} \widehat{\gamma}(h) e^{-2\pi i \omega_j h} \end{aligned} \tag{4.22}$$

where we have put $h = t - s$, with $\widehat{\gamma}(h)$ as given in (1.34).[7]

Recall, $P(\omega_j) = (4/n) I(\omega_j)$ where $P(\omega_j)$ is the scaled periodogram defined in (4.6). Henceforth we will work with $I(\omega_j)$ instead of $P(\omega_j)$. In view of (4.22), the periodogram, $I(\omega_j)$, is the sample version of $f(\omega_j)$ given in (4.12). That is, we may think of the periodogram as the "sample spectral density" of x_t.

It is sometimes useful to work with the real and imaginary parts of the DFT individually. To this end, we define the following transforms.

Definition 4.3 *Given data* $x_1, \ldots, x_n$, *we define the* **cosine transform**

$$d_c(\omega_j) = n^{-1/2} \sum_{t=1}^{n} x_t \cos(2\pi\omega_j t) \tag{4.23}$$

and the **sine transform**

$$d_s(\omega_j) = n^{-1/2} \sum_{t=1}^{n} x_t \sin(2\pi\omega_j t) \tag{4.24}$$

where $\omega_j = j/n$ *for* $j = 0, 1, \ldots, n-1$.

We note that $d(\omega_j) = d_c(\omega_j) - i\, d_s(\omega_j)$ and hence

$$I(\omega_j) = d_c^2(\omega_j) + d_s^2(\omega_j). \tag{4.25}$$

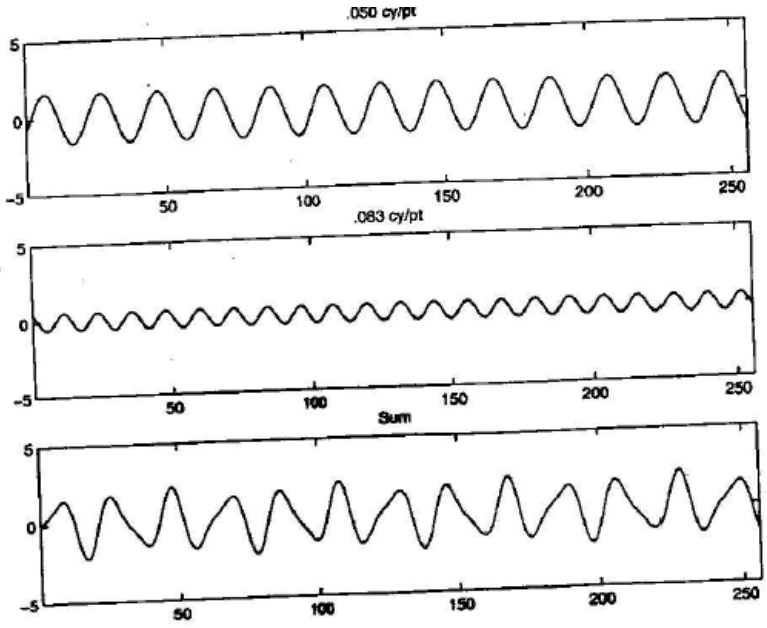

Figure 3.1: Periodic components with periods 20 and 12 points, respectively, and linear combination (bottom panel) corresponding to the model (3.3) with $q = 2$.

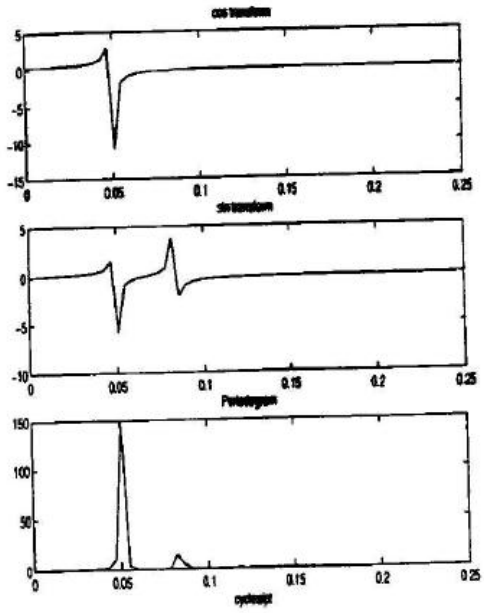

Figure 3.6: Cosine transform, sine transform, and periodogram of a periodic random series.

Example 4.1 A Periodic Series

Figure 4.1 shows an example of the mixture (4.3) with $q = 3$ constructed in the following way. First, for $t = 1, \ldots, 100$, we generated three series

$$x_{t1} = 2\cos(2\pi t\, 6/100) + 3\sin(2\pi t\, 6/100)$$
$$x_{t2} = 4\cos(2\pi t\, 10/100) + 5\sin(2\pi t\, 10/100)$$
$$x_{t3} = 6\cos(2\pi t\, 40/100) + 7\sin(2\pi t\, 40/100)$$

These three series are displayed in Figure 4.1 along with the corresponding frequencies and squared amplitudes. For example, the squared amplitude of x_{t1} is $A^2 = 2^2 + 3^2 = 13$. Hence, the maximum and minimum values that x_{t1} will attain are $\pm\sqrt{13} = \pm 3.61$.

Finally, we constructed

$$x_t = x_{t1} + x_{t2} + x_{t3}$$

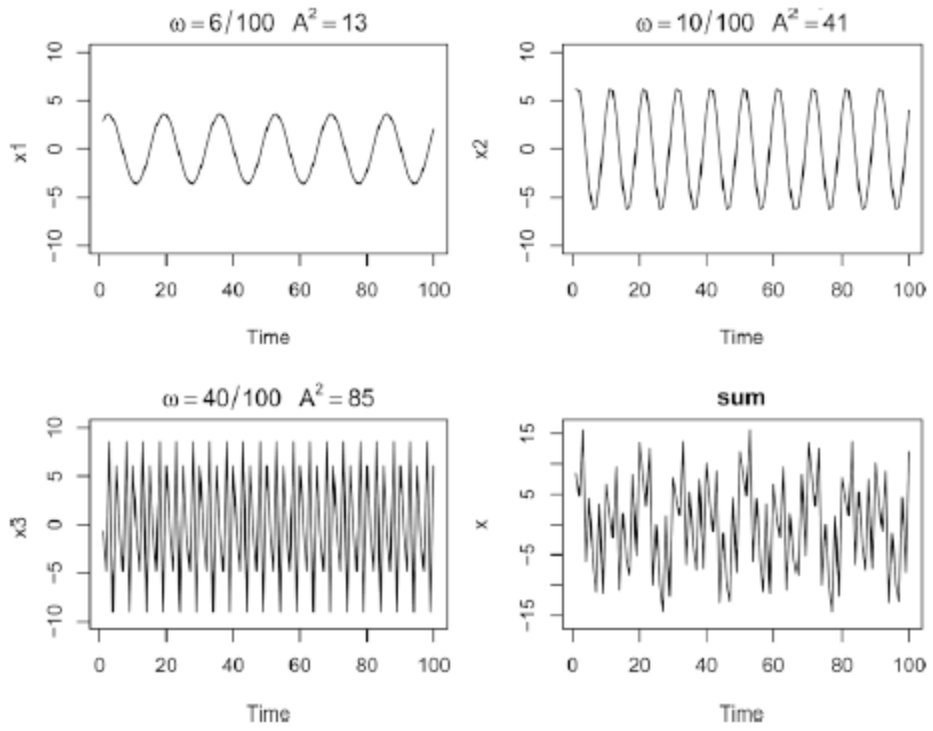

Fig. 4.1. Periodic components and their sum as described in Example 4.1.

Example 4.2 The Scaled Periodogram for Example 4.1

In §2.3, Example 2.9, we introduced the periodogram as a way to discover the periodic components of a time series. Recall that the scaled periodogram is given by

$$P(j/n) = \left(\frac{2}{n}\sum_{t=1}^{n} x_t \cos(2\pi t j/n)\right)^2 + \left(\frac{2}{n}\sum_{t=1}^{n} x_t \sin(2\pi t j/n)\right)^2, \quad (4.6)$$

and it may be regarded as a measure of the squared correlation of the data with sinusoids oscillating at a frequency of $\omega_j = j/n$, or j cycles in n time points. Recall that we are basically computing the regression of the data on the sinusoids varying at the fundamental frequencies, j/n. As discussed in Example 2.9, the periodogram may be computed quickly using the fast Fourier transform (FFT), and there is no need to run repeated regressions.

The scaled periodogram of the data, x_t, simulated in Example 4.1 is shown in Figure 4.2, and it clearly identifies the three components x_{t1}, x_{t2}, and x_{t3} of x_t. Note that

$$P(j/n) = P(1 - j/n), \quad j = 0, 1, \ldots, n-1,$$

so there is a mirroring effect at the folding frequency of 1/2; consequently, the periodogram is typically not plotted for frequencies higher than the folding frequency. In addition, note that the heights of the scaled periodogram shown in the figure are

$$P(6/100) = 13, \quad P(10/100) = 41, \quad P(40/100) = 85,$$

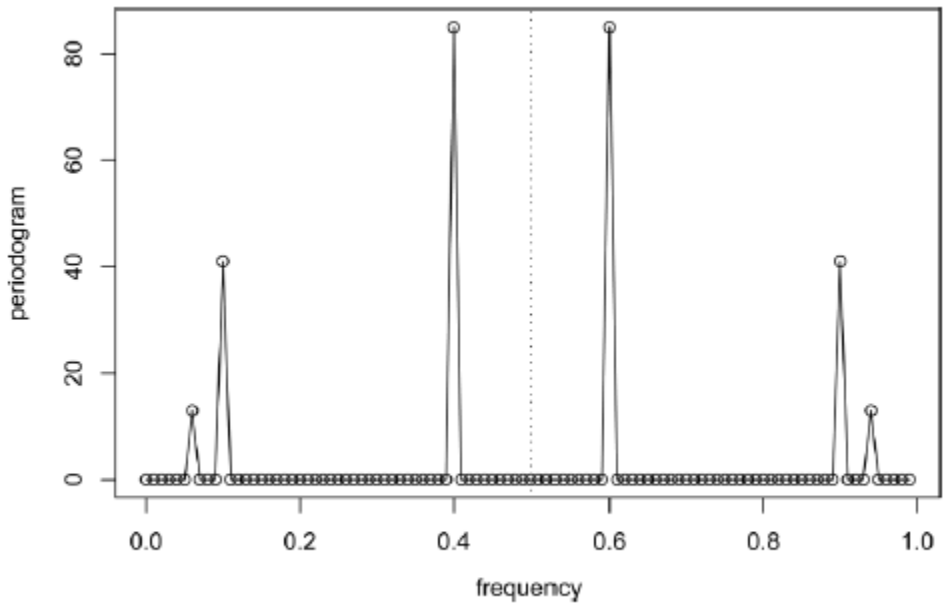

Fig. 4.2. Periodogram of the data generated in Example 4.1.

Large sample properties of the periodogram.

First, let μ be the mean of a stationary process x_t with absolutely summable autocovariance function $\gamma(h)$ and spectral density $f(\omega)$. We can use the same argument as in (4.22), replacing $\bar{x}$ by μ in (4.21), to write

$$I(\omega_j) = n^{-1} \sum_{h=-(n-1)}^{n-1} \sum_{t=1}^{n-|h|} (x_{t+|h|} - \mu)(x_t - \mu) e^{-2\pi i \omega_j h} \tag{4.27}$$

where ω_j is a non-zero fundamental frequency. Taking expectation in (4.27) we obtain

$$E\left[I(\omega_j)\right] = \sum_{h=-(n-1)}^{n-1} \left(\frac{n-|h|}{n}\right) \gamma(h) e^{-2\pi i \omega_j h}. \tag{4.28}$$

For any given $\omega \neq 0$, choose a sequence of fundamental frequencies $\omega_{j:n} \to \omega$[8] from which it follows by (4.28) that, as $n \to \infty$[9]

$$E\left[I(\omega_{j:n})\right] \to f(\omega) = \sum_{h=-\infty}^{\infty} \gamma(h) e^{-2\pi i h \omega}. \tag{4.29}$$

[8] By this we mean $\omega_{j:n} = j_n/n$, where $\{j_n\}$ is a sequence of integers chosen so that j_n/n is the closest Fourier frequency to ω; consequently, $|j_n/n - \omega| \leq \frac{1}{2n}$.

[9] From Definition 4.2 we have $I(0) = n\bar{x}^2$, so the analogous result of (4.29) for the case $\omega = 0$ is $E[I(0)] - n\mu^2 = n\,\mathrm{var}(\bar{x}) \to f(0)$ as $n \to \infty$.

To examine the asymptotic distribution of the periodogram, we note that if x_t is a normal time series, the sine and cosine transforms will also be jointly normal, because they are linear combinations of the jointly normal random variables $x_1, x_2, \ldots, x_n$. In that case, the assumption that the covariance function satisfies the condition

$$\theta = \sum_{h=-\infty}^{\infty} |h||\gamma(h)| \ < \infty \tag{4.30}$$

is enough to obtain simple large sample approximations for the variances and covariances. Using the same argument used to develop (4.28) we have

$$\mathrm{cov}[d_c(\omega_j), d_c(\omega_k)] = n^{-1} \sum_{s=1}^{n} \sum_{t=1}^{n} \gamma(s-t) \cos(2\pi\omega_j s) \cos(2\pi\omega_k t), \tag{4.31}$$

$$\mathrm{cov}[d_c(\omega_j), d_s(\omega_k)] = n^{-1} \sum_{s=1}^{n} \sum_{t=1}^{n} \gamma(s-t) \cos(2\pi\omega_j s) \sin(2\pi\omega_k t), \tag{4.32}$$

and

$$\mathrm{cov}[d_s(\omega_j), d_s(\omega_k)] = n^{-1} \sum_{s=1}^{n} \sum_{t=1}^{n} \gamma(s-t) \sin(2\pi\omega_j s) \sin(2\pi\omega_k t), \tag{4.33}$$

where the variance terms are obtained by setting $\omega_j = \omega_k$ in (4.31) and (4.33).

under assumption (4.30), namely, for $\omega_j, \omega_k \neq 0$ or $1/2$,

$$\mathrm{cov}[d_c(\omega_j), d_c(\omega_k)] = \begin{cases} f(\omega_j)/2 + \varepsilon_n & \omega_j = \omega_k, \\ \varepsilon_n & \omega_j \neq \omega_k, \end{cases} \tag{4.34}$$

$$\mathrm{cov}[d_s(\omega_j), d_s(\omega_k)] = \begin{cases} f(\omega_j)/2 + \varepsilon_n & \omega_j = \omega_k, \\ \varepsilon_n & \omega_j \neq \omega_k, \end{cases} \tag{4.35}$$

and

$$\mathrm{cov}[d_c(\omega_j), d_s(\omega_k)] = \varepsilon_n, \tag{4.36}$$

where the error term ε_n in the approximations can be bounded,

$$|\varepsilon_n| \leq \theta/n, \tag{4.37}$$

and θ is given by (4.30). If $\omega_j = \omega_k = 0$ or $1/2$ in (4.34), the multiplier $1/2$ disappears; note that $d_s(0) = d_s(1/2) = 0$, so (4.35) does not apply.

Example 4.9 Covariance of Sine and Cosine Transforms

For the three-point moving average series of Example 1.9 and $n = 256$ observations, the theoretical covariance matrix of the vector $\boldsymbol{d} = (d_c(\omega_{26}), d_s(\omega_{26}), d_c(\omega_{27}), d_s(\omega_{27}))'$ is

$$\mathrm{cov}(\boldsymbol{d}) = \begin{pmatrix} .3752 & -.0009 & -.0022 & -.0010 \\ -.0009 & .3777 & -.0009 & .0003 \\ -.0022 & -.0009 & .3667 & -.0010 \\ -.0010 & .0003 & -.0010 & .3692 \end{pmatrix}.$$

The diagonal elements can be compared with half the theoretical spectral values of $\frac{1}{2}f(\omega_{26}) = .3774$ for the spectrum at frequency $\omega_{26} = 26/256$, and of $\frac{1}{2}f(\omega_{27}) = .3689$ for the spectrum at $\omega_{27} = 27/256$. Hence, the cosine and sine transforms produce nearly uncorrelated variables with variances approximately equal to one half of the theoretical spectrum. For this particular case, the uniform bound is determined from $\theta = 8/9$, yielding $|\varepsilon_{256}| \leq .0035$ for the bound on the approximation error.

If $x_t \sim \mathrm{iid}(0, \sigma^2)$, then it follows from (4.30)-(4.36), Problem 2.10(d), and a central limit theorem[10] that

$$d_c(\omega_{j:n}) \sim \mathrm{AN}(0, \sigma^2/2) \quad \text{and} \quad d_s(\omega_{j:n}) \sim \mathrm{AN}(0, \sigma^2/2) \tag{4.38}$$

jointly and independently, and independent of $d_c(\omega_{k:n})$ and $d_s(\omega_{k:n})$ provided $\omega_{j:n} \to \omega_1$ and $\omega_{k:n} \to \omega_2$ where $0 < \omega_1 \neq \omega_2 < 1/2$. We note that in this case, $f_x(\omega) = \sigma^2$. In view of (4.38), it follows immediately that as $n \to \infty$,

$$\frac{2I(\omega_{j:n})}{\sigma^2} \xrightarrow{d} \chi^2_2 \quad \text{and} \quad \frac{2I(\omega_{k:n})}{\sigma^2} \xrightarrow{d} \chi^2_2 \tag{4.39}$$

with $I(\omega_{j:n})$ and $I(\omega_{k:n})$ being asymptotically independent, where χ^2_ν denotes a chi-squared random variable with ν degrees of freedom.

Property 4.4 Distribution of the Periodogram Ordinates

If

$$x_t = \sum_{j=-\infty}^{\infty} \psi_j w_{t-j}, \qquad \sum_{j=-\infty}^{\infty} |\psi_j| < \infty \tag{4.40}$$

where $w_t \sim iid(0, \sigma_w^2)$*, and (4.30) holds, then for any collection of* m *distinct frequencies* $\omega_j \in (0, 1/2)$ *with* $\omega_{j:n} \to \omega_j$

$$\frac{2I(\omega_{j:n})}{f(\omega_j)} \xrightarrow{d} \text{iid } \chi_2^2 \tag{4.41}$$

provided $f(\omega_j) > 0$*, for* $j = 1, \ldots, m$.

This result is stated more precisely in Theorem C.7 of §C.3. Other approaches to large sample normality of the periodogram ordinates are in terms of cumulants, as in Brillinger (1981), or in terms of mixing conditions, such as in Rosenblatt (1956a). Here, we adopt the approach used by Hannan (1970), Fuller (1996), and Brockwell and Davis (1991).

The distributional result (4.41) can be used to derive an approximate confidence interval for the spectrum in the usual way. Let $\chi_\nu^2(\alpha)$ denote the lower α probability tail for the chi-squared distribution with ν degrees of freedom; that is,

$$\Pr\{\chi_\nu^2 \le \chi_\nu^2(\alpha)\} = \alpha. \tag{4.42}$$

Then, an approximate $100(1-\alpha)\%$ confidence interval for the spectral density function would be of the form

$$\frac{2\ I(\omega_{j:n})}{\chi_2^2(1-\alpha/2)} \le f(\omega) \le \frac{2\ I(\omega_{j:n})}{\chi_2^2(\alpha/2)}. \tag{4.43}$$

Example 1.5 El Niño and Fish Population

We may also be interested in analyzing several time series at once. Figure 1.5 shows monthly values of an environmental series called the Southern Oscillation Index (SOI) and associated Recruitment (number of new fish) furnished by Dr. Roy Mendelssohn of the Pacific Environmental Fisheries Group (personal communication). Both series are for a period of 453 months ranging over the years 1950–1987. The SOI measures changes in air pressure, related to sea surface temperatures in the central Pacific Ocean. The central Pacific warms every three to seven years due to the El Niño effect, which has been blamed, in particular, for the 1997 floods in the midwestern portions of the United States. Both series in Figure 1.5 tend to exhibit repetitive behavior, with regularly repeating cycles that are easily visible. This periodic behavior is of interest because underlying processes of interest may be regular and the rate or frequency of oscillation characterizing the behavior of the underlying series would help to identify them. One can also remark that the cycles of the SOI are repeating at a faster rate than those of the Recruitment series. The Recruitment series also shows several kinds of oscillations, a faster frequency that seems to repeat about every 12 months and a slower frequency that seems to repeat about every 50 months.

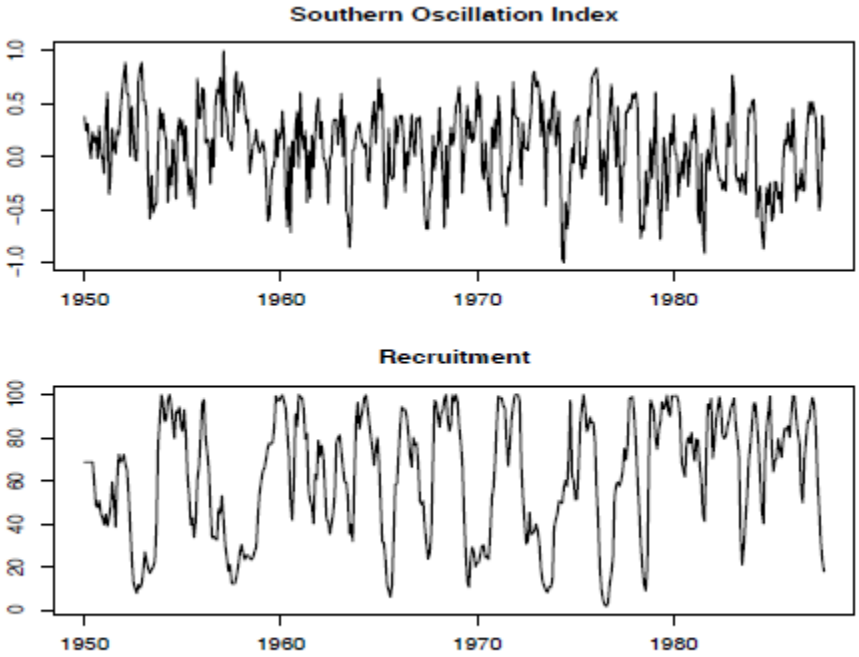

Fig. 1.5. Monthly SOI and Recruitment (estimated new fish), 1950-1987.

Example 4.10 Periodogram of SOI and Recruitment Series

Figure 4.4 shows the periodograms of each series, where the frequency axis is labeled in multiples of $\Delta = 1/12$. As previously indicated, the centered data have been padded to a series of length 480. We notice a narrow-band peak at the obvious yearly (12 month) cycle, $\omega = 1\Delta = 1/12$. In addition, there is considerable power in a wide band at the lower frequencies that is centered around the four-year (48 month) cycle $\omega = \frac{1}{4}\Delta = 1/48$ representing a possible El Niño effect. This wide band activity suggests that the possible El Niño cycle is irregular, but tends to be around four years on average. We will continue to address this problem as we move to more sophisticated analyses.

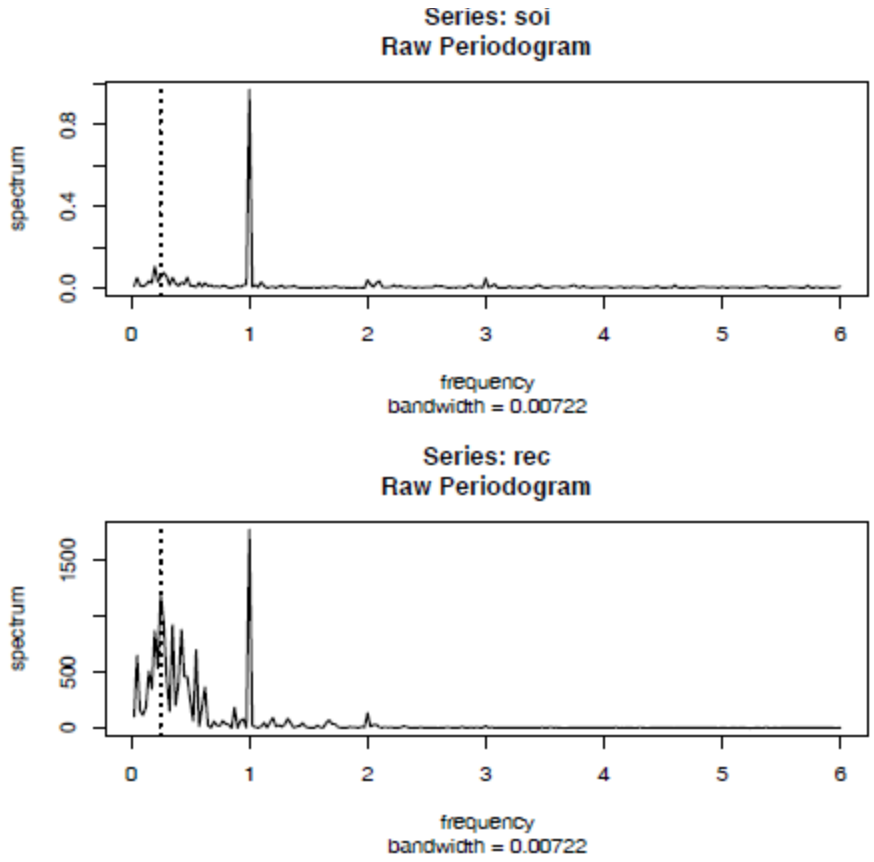

Fig. 4.4. Periodogram of SOI and Recruitment, $n = 453$ ($n' = 480$), where the frequency axis is labeled in multiples of $\Delta = 1/12$. Note the common peaks at $\omega = 1\Delta = 1/12$, or one cycle per year (12 months), and $\omega = \frac{1}{4}\Delta = 1/48$, or one cycle every four years (48 months).

Noting $\chi^2_2(.025) = .05$ and $\chi^2_2(.975) = 7.38$, we can obtain approximate 95% confidence intervals for the frequencies of interest. For example, the periodogram of the SOI series is $I_S(1/12) = .97$ at the yearly cycle. An approximate 95% confidence interval for the spectrum $f_S(1/12)$ is then

$$[2(.97)/7.38,\ 2(.97)/.05] = [.26,\ 38.4],$$

which is too wide to be of much use. We do notice, however, that the lower value of .26 is higher than any other periodogram ordinate, so it is safe to say that this value is significant. On the other hand, an approximate 95% confidence interval for the spectrum at the four-year cycle, $f_S(1/48)$, is

$$[2(.05)/7.38,\ 2(.05)/.05] = [.01,\ 2.12],$$

which again is extremely wide, and with which we are unable to establish significance of the peak.

The example above makes it clear that the periodogram as an estimator is susceptible to large uncertainties, and we need to find a way to reduce the variance.